Transition radiation from relativistic electrons in periodic radiators*

Michael L. Cherry, Gernot Hartmann,† Dietrich Müller, and Thomas A. Prince
Enrico Fermi Institute and Department of Physics, University of Chicago, Chicago, Illinois 60637
(Received 29 July 1974)

The generation and detection of transition radiation have been studied in a series of experiments with electrons from 1 to 15 GeV at SLAC and at the Cornell Synchrotron. Periodic radiators, consisting of thin plastic foils stretched in air at constant spacings, were used, and proportional chambers filled with krypton or xenon served as detectors. A detailed discussion of the theoretical predictions is given, and the measurements are systematically compared with the predictions by varying the most critical parameters, such as configuration of radiators and detectors, and energy of the electrons. In general, good agreement between theory and experiment has been found. On the basis of these results, the criteria are summarized under which transition radiation can readily be observed.

I. INTRODUCTION

The phenomenon of transition radiation, that is, the generation of photons when an energetic particle traverses the interface between two media, has recently raised considerable interest. This interest has not only been centered on studies of the effect itself, but it has also been strongly stimulated by challenging applications of this phenomenon in high-energy physics and cosmic-ray research. In particular, the identification of highly relativistic particles by means of transition-radiation detectors has become a much debated possibility.

The mechanism of transition radiation has been proposed and investigated in extensive theoretical studies since 1946.[1-3] Due to the low intensity of the radiation, experimental evidence was found much later,[4-7] and only recently has the *efficient* detection of transition radiation in the x-ray regime become possible.[8-11] Still, the available amount of theoretical detail by far exceeds the existing experimental data. Many aspects of the theory have not yet been verified by measurements. Furthermore, the large number of parameters, which may have strong effects on the detectable radiation yield, leads to some confusion with respect to the design of practical transition-radiation detectors.

To help clarify this situation, we have performed a series of experiments with electrons of 1–15 GeV at the SLAC and Cornell accelerators, and in this paper we shall present a summary of the results obtained with a variety of experimental configurations. In particular, we shall systematically compare our measurements with the predictions of the theory. For this purpose, we shall also summarize those theoretical details which seem to be most important for experimental work. Finally, as a simple guideline for experiments, we shall derive from our measurements and calculations a set of rules which should be followed in order to make transition radiation observable and usable for practical purposes.

A second goal of our experiments was the study of transition-radiation detectors for a specific application, namely the efficient identification and discrimination of relativistic particles in cosmic-ray and high-energy work. Preliminary results of this aspect have already been published.[11]

II. SUMMARY OF THE THEORETICAL PREDICTIONS

Many aspects of the theory of transition radiation have been worked out in numerous publications (for an extensive bibliography see Ter-Mikaelian[12]). However, it is sometimes quite difficult to extract the characteristic features which are most important for experimental work. In the following we shall therefore give a brief discussion of those theoretical predictions which apply to measurements such as ours. We shall first discuss the single-interface formulas, which are the basis of the theory and can in certain cases be used to estimate the magnitude of the effect in more complicated configurations. Next the complications will be examined which arise when transition radiation is generated in a periodic radiator consisting of many interfaces. We shall restrict ourselves to the case of highly relativistic particles with $\gamma = E/mc^2 \gg 1$.

A. Single interface

The frequency spectrum of transition radiation emitted by a particle with charge e upon perpendicular traversal through a *single* interface between two media with dielectric constants ϵ_1 and ϵ_2 has been calculated by Ginzburg and Frank,[1] and by Garibian.[2,13] These calculations show that for highly relativistic particles most of the radiation is emitted in the x-ray region. With $\epsilon_{1,2} = 1 - \omega_{1,2}^2/\omega^2$

(where $\omega_{1,2}$ are the plasma frequencies of the two media), relatively simple expressions have been found for the differential and the total radiation intensities:

$$\frac{d^2S_0}{d\theta d\omega} = \frac{2\alpha\hbar\theta^3}{\pi}\left(\frac{1}{1/\gamma^2+\theta^2+\omega_1^2/\omega^2} - \frac{1}{1/\gamma^2+\theta^2+\omega_2^2/\omega^2}\right)^2, \tag{1a}$$

$$\frac{dS_0}{d\omega} = \frac{\alpha\hbar}{\pi}\left[\left(\frac{\omega_1^2+\omega_2^2+2\omega^2/\gamma^2}{\omega_1^2-\omega_2^2}\right) \times \ln\left(\frac{1/\gamma^2+\omega_1^2/\omega^2}{1/\gamma^2+\omega_2^2/\omega^2}\right)-2\right], \tag{1b}$$

$$S_0 = \int\int\left(\frac{d^2S_0}{d\theta d\omega}\right)d\theta\, d\omega = \frac{\alpha\hbar}{3}\frac{(\omega_1-\omega_2)^2}{\omega_1+\omega_2}\gamma, \tag{1c}$$

where ω = photon frequency, θ = emission angle of the photon with respect to the particle trajectory, and $\alpha = e^2/\hbar c$.

The radiation is sharply peaked in the forward direction at an angle $\theta \approx (1/\gamma^2+\omega_2^2/\omega^2)^{1/2}$ [Eq. (1a), with the assumption $\omega_1 > \omega_2$, an assumption which is used throughout this paper]. Equation (1b) describing the differential energy spectrum can be broken up in essentially three regions having respectively, constant, logarithmic, and power-law dependence on ω and γ:

$$\frac{dS_0}{d\omega} \approx \begin{cases} \frac{2\alpha\hbar}{\pi}\left(\ln\frac{\omega_1}{\omega_2}-1\right), & \omega < \gamma\omega_2 \quad (2a) \\ \frac{2\alpha\hbar}{\pi}\ln\frac{\gamma\omega_1}{\omega}, & \gamma\omega_2 < \omega < \gamma\omega_1 \quad (2b) \\ \frac{\alpha\hbar}{6\pi}\left(\frac{\gamma\omega_1}{\omega}\right)^4, & \gamma\omega_1 < \omega\,. \quad (2c) \end{cases}$$

At frequencies exceeding a "cutoff" frequency $\omega = \gamma\omega_1$, the radiation intensity drops rapidly to very small values. An example of the spectrum (1b) is shown in Fig. 1.

The most appealing feature of transition radiation seems to be its dependence on the Lorentz factor γ of the particle: The total intensity [Eq. (1c)] increases linearly with γ, essentially due to the fact that the photon spectrum becomes harder with increasing γ. It should be noted, however, that measurements with detectors which are only sensitive in a limited frequency interval would, in general, not follow a linear γ dependence, but develop into a logarithmic behavior [Eq. (2b)] and eventually reach saturation [when $\gamma > \omega/\omega_2$, Eq. (2a)]. The logarithmic dependence would persist for large values of γ only if one of the two media were vacuum ($\omega_2 = 0$).

B. Periodic radiator

Complications arise due to the fact that the transition radiation generated at a single interface can in general not be observed. In practice, the particle traverses at least two interfaces of a slab of material. Furthermore, since the total radiation yield per interface is very small [$S_0 \approx 10^{-2}\gamma$ eV, Eq. (1c)], the effect should be enhanced for experimental studies. A radiator may be chosen in which the particle traverses many interfaces, for instance, a stack of thin foils of low-Z material, stretched in air at constant spacings. In this case, interference effects between the individual interfaces of the radiator must be taken into account, leading to a modulation of the frequency distribution obtained from a single interface, and, for high values of γ, to a saturation of the yield. The differential spectrum of x-ray transition radiation for a periodic radiator of N foils with thickness l_1 and spacing l_2 is given by

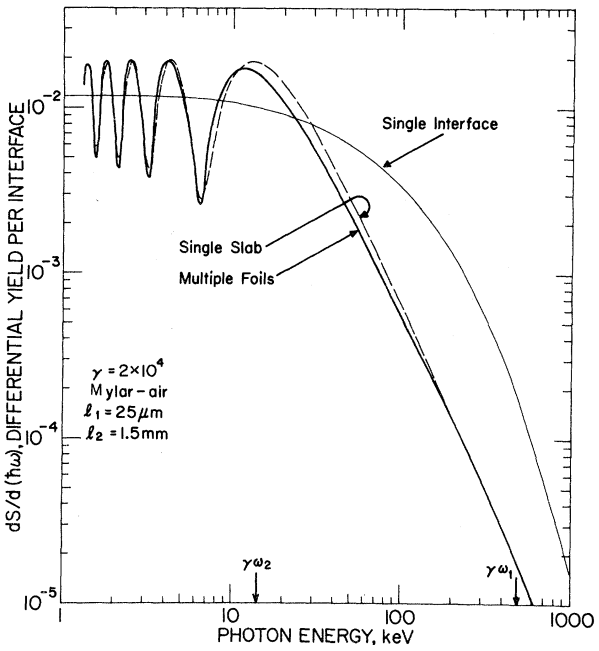

FIG. 1. Comparison of $dS/d(\hbar\omega)$, the computed differential yield (keV/keV) per interface, as a function of $\hbar\omega$, the photon energy, for different Mylar-air radiators. For a single interface (thin line), $dS/d(\hbar\omega) = dS_0/d(\hbar\omega)$; for a single slab (thickness $l_1 = 25\,\mu$m, dashed line), $dS/d(\hbar\omega) = \frac{1}{2}\,dS_1/d(\hbar\omega)$; and for multiple foils (thickness $l_1 = 25\,\mu$m and spacing $l_2 = 1.5$ mm, heavy line), $dS/d(\hbar\omega) = (1/2N)dS_N/d(\hbar\omega)$. The particle energy is $\gamma = 2\times 10^4$.

$$\frac{d^2S_N}{d\theta d\omega} = \frac{d^2S_0}{d\theta d\omega} 4\sin^2\left(\frac{l_1}{Z_1}\right) \frac{\sin^2[N(l_1/Z_1 + l_2/Z_2)]}{\sin^2(l_1/Z_1 + l_2/Z_2)}, \tag{3a}$$

where Z_1 and Z_2 are the "formation zones" for the two media:

$$Z_{1,2} = \frac{4c}{\omega}\left(\frac{1}{\gamma^2} + \theta^2 + \frac{\omega_{1,2}^2}{\omega^2}\right)^{-1}. \tag{3b}$$

Physically, the formation zone is the distance along the particle trajectory in a given medium after which the separation between particle and generated photon is of the order of the photon wavelength.

As shown in the Appendix, expression (3a) can be simply obtained by linear superposition of the single-interface expressions [Eq. (1)], taking the phase relations between the individual interfaces properly into account. Earlier derivations of Eq. (3a) by different approaches have been given by Ter-Mikaelian[3] and by Garibian.[14] In the following, we shall discuss the consequences of Eq. (3a) in some detail.

For the case $N=1$, we obtain the radiation yield of a single slab of material:

$$\frac{d^2S_1}{d\theta d\omega} = \frac{d^2S_0}{d\theta d\omega} 4\sin^2\left(\frac{l_1}{Z_1}\right). \tag{4}$$

From an experimental viewpoint, it is interesting to determine the conditions for which the yield from a single slab is comparable to that from two single interfaces. To this end, we consider a detector which has frequency resolution $\Delta\omega$, angular resolution $\Delta\theta$, and uniform response over $\Delta\omega$ and $\Delta\theta$. The *observed* differential spectrum is then the spectrum of Eq. (4), averaged over $\Delta\theta$ and $\Delta\omega$. If the thickness of the foil exceeds the formation zone for the foil material,

$$l_1 \gg Z_1(\theta, \omega),$$

then the term $\sin^2(l_1/Z_1)$ in Eq. (4) oscillates rapidly as compared to the range in which $d^2S_0/d\theta d\omega$ varies considerably. If it also oscillates rapidly as compared to the resolution of the detector, then the average over $\Delta\theta$ and $\Delta\omega$ is

$$\left\langle \frac{d^2S_1}{d\theta d\omega} \right\rangle_{\Delta\theta,\,\Delta\omega} = \frac{1}{\Delta\theta\Delta\omega}\int_{\Delta\theta}\int_{\Delta\omega}\left(\frac{d^2S_1}{d\theta' d\omega'}\right) d\theta' d\omega'$$
$$= \left\langle \frac{d^2S_0}{d\theta d\omega} \right\rangle_{\Delta\theta,\,\Delta\omega} \left\langle 4\sin^2\frac{l_1}{Z_1} \right\rangle_{\Delta\theta,\,\Delta\omega},$$

and since

$$\langle \sin^2(l_1/Z_1)\rangle_{\Delta\theta,\,\Delta\omega} \approx \tfrac{1}{2}$$

the observed yield is twice that of a single interface.

Returning to the general form for a periodic radiator [Eq. (3a)], we consider now the case $l_2 > Z_2(\theta, \omega)$, i.e., the spacing of the foils exceeds the formation zone of the gap material. In this case, the period of the term

$$\frac{\sin^2[N(l_1/Z_1 + l_2/Z_2)]}{\sin^2(l_1/Z_1 + l_2/Z_2)}$$

is very small compared to the range in which $d^2S_0/d\theta d\omega$ varies. If it is also small compared to the detector resolution, then we may replace the last term in Eq. (3a) by its average[15]:

$$\left\langle \frac{\sin^2[N(l_1/Z_1 + l_2/Z_2)]}{\sin^2(l_1/Z_1 + l_2/Z_2)} \right\rangle_{\Delta\theta,\,\Delta\omega} \approx N. \tag{5}$$

Thus, the observed yield in this case is well approximated by N times the radiation yield of a single slab.

In the opposite case, i.e., when the foil spacing l_2 is smaller than the formation zone Z_2, i.e., $l_2 < Z_2(\theta, \omega)$, the approximation (5) cannot be used even if $l_1 \gg Z_1$. In general, for $l_2 < Z_2$, a reduction of the total yield per interface occurs as compared to N single slabs, until, as the foil spacing approaches zero ($l_2 \to 0$), the radiation yield corresponds to that of a single slab with thickness Nl_1.

The integration of Eq. (3a) over angles[16] has been performed by Ter-Mikaelian[3] and by Garibian[14]:

$$\frac{dS_N}{d\omega} = 2\alpha\hbar c N(\omega_1^2 - \omega_2^2)^2 \frac{(l_1 + l_2)^2}{\omega^2}$$
$$\times \sum_{r=r_{\min}}^{r_{\max}} \left\{ \sin^2\left[\frac{l_2}{l_1 + l_2}\left(\frac{l_1}{4\omega c}(\omega_1^2 - \omega_2^2) - \pi r\right)\right] \frac{2\pi c r - \frac{(l_1 + l_2)\omega}{2\gamma^2} - \frac{l_1\omega_1^2 + l_2\omega_2^2}{2\omega}}{\left[\frac{l_1(\omega_1^2 - \omega_2^2)}{2\omega} - 2\pi c r\right]^2 \left[\frac{l_2(\omega_2^2 - \omega_1^2)}{2\omega} - 2\pi c r\right]^2} \right\}. \tag{6a}$$

The summation is performed over all integer numbers r within the limits $r_{\min} \leq r \leq r_{\max}$, where

$$r_{\min} = \frac{l_1 + l_2}{2\pi\gamma c}\left(\frac{l_1\omega_1^2 + l_2\omega_2^2}{l_1 + l_2}\right)^{1/2}, \tag{6b}$$

$$r_{\max} = \gamma r_{\min}.$$

For each value of r, Eq. (6a) must be evaluated only in a specified frequency region:

$$\gamma^2\left\{\frac{2\pi cr}{l_1+l_2}+\left[\left(\frac{2\pi cr}{l_1+l_2}\right)^2-\frac{l_1\omega_1^2+l_2\omega_2^2}{\gamma^2(l_1+l_2)}\right]^{1/2}\right\}\geq\omega\geq\gamma^2\left\{\frac{2\pi cr}{l_1+l_2}-\left[\left(\frac{2\pi cr}{l_1+l_2}\right)^2-\frac{l_1\omega_1^2+l_2\omega_2^2}{\gamma^2(l_1+l_2)}\right]^{1/2}\right\}. \quad (6c)$$

Most of the contribution to Eq. (6a) comes from the values of r near $r_{\min}$.

For comparison, we have plotted in Fig. 1 and Fig. 2 the radiation yield per interface predicted by Eqs. (1b) and (6a) for Mylar-air interfaces, as used in our experiments. Inspection of the figures leads to the following qualitative conclusions:

(a) The energy spectrum of transition radiation for a periodic radiator is characterized by oscillations of sizable amplitude around the spectrum for a single interface. Maxima of intensity occur (below $\omega=\gamma\omega_1$) at characteristic frequencies $\omega_{m,r}$:

$$\omega_{m,r}=\frac{(\omega_1^2-\omega_2^2)l_1l_2}{2\pi c(l_1+l_2)[(2rl_2)/(l_1+l_2)-2m+1]}. \quad (7)$$

[m are all integer numbers chosen such that $\omega_{m,r}$ fulfills condition (6c).]

(b) For the case shown in Fig. 1, the complication introduced by the expression for a periodic medium over the single slab formula does not result in a major difference in the calculated yield. This is due to the fact that in this case the condition $l_2\gtrsim Z_2$ is fulfilled, i.e., the air formation zone does not significantly exceed the foil spacing.

(c) Most importantly, with increasing particle energy the radiation spectrum of a periodic radiator [Eq. (6a)] does not become harder at the same rate as the single-interface radiation [Eq. (1b)]. This is demonstrated in Fig. 2 where we compare the computed differential yield for both cases at several different energies. As a result, the linear γ dependence of the total radiation yield predicted by Eq. (1c) will not persist for periodic radiators; rather, as shown in Fig. 3, saturation will set in at large γ values. This saturation exists even in the case of a single slab. It follows from Eq. (6) that saturation will be reached when the largest frequency ω contributing to the $r=1$ term equals the "cutoff" energy $\gamma\omega_1$. This defines a "saturation energy" γ_s:

$$\gamma_s=\frac{1}{4\pi c}\left[(l_1+l_2)\omega_1+\frac{1}{\omega_1}(l_1\omega_1^2+l_2\omega_2^2)\right]. \quad (8)$$

The frequency spectrum of transition radiation as discussed thus far characterizes the x-ray yield generated in the radiator without considering reabsorption. However, reabsorption does strongly suppress the radiation intensity emerging from a radiator at low x-ray energies. This is demonstrated in Fig. 4 where we show the net spectrum computed for a typical radiator, taking tabulated absorption cross sections[17-19] into account and assuming that x rays are generated according to Eq. (6a) with equal probability anywhere within the radiator.

Figures 1, 2, and 4 demonstrate that most of the generated radiation occurs with frequencies around the last maximum in the differential frequency spectrum, that is, at the highest value of $\omega_{m,r}$ [see Eq. (7)] which is allowed under the condition $\omega_{m,r}<\gamma\omega_1$. This effect is enhanced by the suppression of low x-ray frequencies due to absorption (see Fig. 4). As saturation (with increasing γ) is approached, this maximum frequency will be [Eq. (7), with $r=1$, $m=1$]

$$\omega_{\max}\approx\frac{l_1\omega_1^2}{2\pi c} \text{ if } \omega_1\gg\omega_2 \text{ and } l_2\gg l_1, \quad (9)$$

i.e., $\omega_{\max}$ is roughly proportional to the mass density of the individual radiator foils, and it does not depend on the particle energy. It is interesting to note that radiator thickness l_1, frequency $\omega_{\max}$ [Eq. (9)], and formation zone Z_1 are closely related: The formation zone Z_1, evaluated for

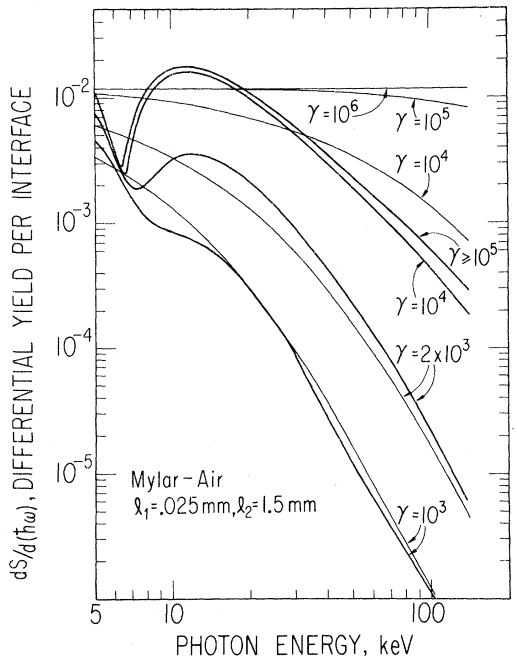

FIG. 2. Comparison of $dS/d(\hbar\omega)$, the differential yield per interface, computed for a single interface (thin lines), and a multifoil radiator (heavy lines) for different energies $\gamma=E/mc^2$.

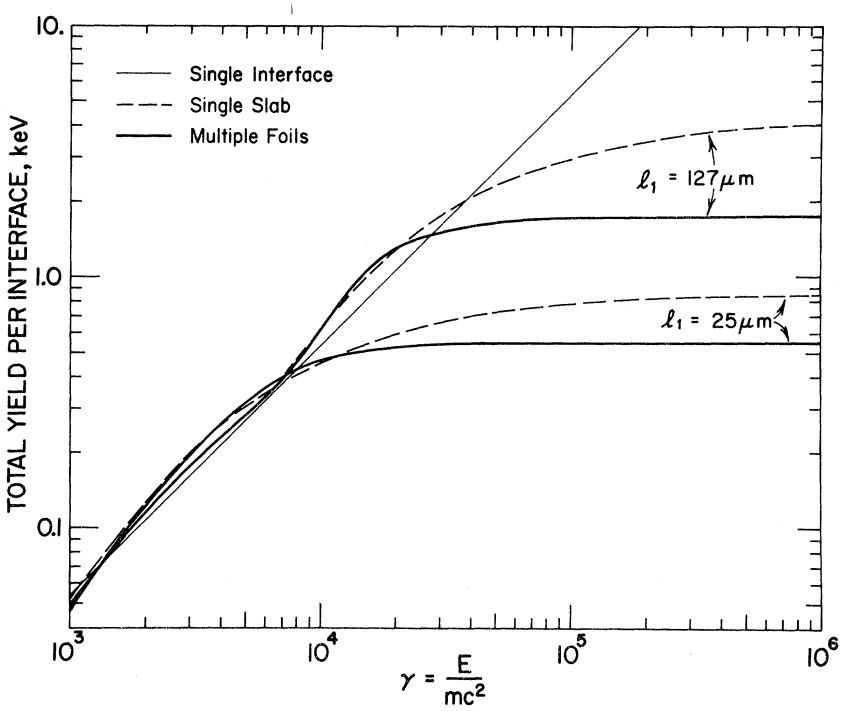

FIG. 3. Comparison of the *total* generated yield per interface, S, as a function of the particle energy $\gamma = E/mc^2$ for single interface (thin line), single slab (dashed line), and multifoil radiator (heavy line). The yield is computed for Mylar-air interfaces, with foil thicknesses $l_1 = 25\ \mu$m and $127\ \mu$m, and spacing $l_2 = 1.5$ mm.

$\omega = \omega_{max}$ (and $\theta \approx 1/\gamma$), approximately equals the thickness l_1, i.e., $Z_1(\omega_{max}) \approx l_1$. Some numerical examples are given in Secs. IV and V.

III. EXPERIMENTAL PROCEDURES

We have investigated the generation of transition radiation by electrons with energies from 1 to 15 GeV at SLAC and at the Cornell Synchrotron. We used radiators consisting of several hundred plastic foils, stretched in air. Multiwire proportional chambers served as detectors. As mentioned, transition-radiation photons propagate essentially along the same trajectory as the particle generating the radiation. Therefore, both the particle and the transition x rays will traverse a detector simultaneously, unless the particle is deflected after passing through the radiator. This latter possibility appears to be impractical for many applications of the effect and has not been used in our experiments. Instead, a detector filled with a gas of high atomic number (xenon or krypton) has been chosen. This seems to be the best compromise if x rays are to be detected efficiently in the presence of the ionization signal of the particle.

The basic arrangement used in the accelerator runs is shown in Fig. 5. The accelerator beam available at SLAC was a secondary beam from a tungsten target ("C beam"), while at the Cornell Synchrotron a photon beam from an internal target, converted in front of a pair spectrometer, was used. At both accelerators, the uncertainty in the electron energy was less than 5%. Several radiators could be placed in the beam, and each radiator was followed by a proportional chamber. Plastic scintillators $S1$, $S2$, $S3$ and anticounters $A1$, $A2$ were used to define the beam: Only events satisfying the fast coincidence condition $S1 \cdot S2 \cdot S3 \cdot \overline{A1} \cdot \overline{A2}$ were accepted. Four radiation lengths of tungsten, followed by scintillator $S4$, served as a shower detector at the downstream end of the apparatus. Thereby, spurious low-energy electrons and, at SLAC, a pion background in the electron beam could be identified and rejected. For each accepted event, the pulses from all proportional chambers as well as from the scintillators $S1$, $S2$, $S4$ were simultaneously and independently fed through charge sensitive amplifiers (CSA) into pulse-height analyzers (PHA), and the data were stored on magnetic tape.

Most radiators consisted of 188 foils of either Mylar ($\hbar\omega_1 = 24.4$ eV) or polypropylene ($\hbar\omega_1 = 20.9$ eV), with constant spacings of air ($\hbar\omega_2 = 0.71$ eV). In addition, in order to define a simple, inexpensive material for large-area detectors, a variety of plastic-foam radiators were

used. Since it is, however, not easily possible to compare the measured yield from foam radiators with calculations, these results will be published separately.[20] In the present paper, we shall restrict ourselves to results obtained with foils.

Figure 6 shows a schematic cross section of a multiwire proportional chamber. The chambers had a sensitive thickness of 4 cm or 2 cm at atmospheric pressure, and were filled with xenon or krypton, with 20% (by volume) of CO_2 added as quencher. Before reaching the sensitive volume, entering particles and x rays had to traverse a thin window (51 μm Mylar), followed by a dead space of 1 mm and by the high-voltage plane (10 μm aluminum). The chambers were operated in a sealed mode. To prevent deterioration due to atmospheric oxygen diffusing through the windows, they were kept in thin plastic bags (13 μm), filled with dry nitrogen or with CO_2. The signals were extracted from the wires, all wires (51 μm stainless steel at 1 cm spacing) being electrically connected for each chamber.

Using tabulated x-ray absorption cross sections,[17-19] we have computed the portion of the transition radiation emitted from a given radiator which we expect to be absorbed in our proportional chambers. As an example, this portion is shown in Fig. 4 for 15-GeV electrons and a 4-cm chamber filled with xenon or krypton, behind a Mylar radiator. This figure demonstrates how well the region of x-ray energies in which the chambers are sensitive matches the spectrum of the emitted transition radiation. Of course, low-energy x rays will be lost by absorption in the material between the radiator and the sensitive chamber region, and at high energies, the chambers will become increasingly transparent. In Sec. IV the expected signals will be systematically compared with the measurements.

During the accelerator runs, we have also regularly performed null measurements for all energies and all multiwire chambers by replacing the radiators with solid Mylar or polypropylene pieces of equivalent thickness. In this manner we made sure that transition radiation was indeed generated by the laminated radiator structure and not simu-

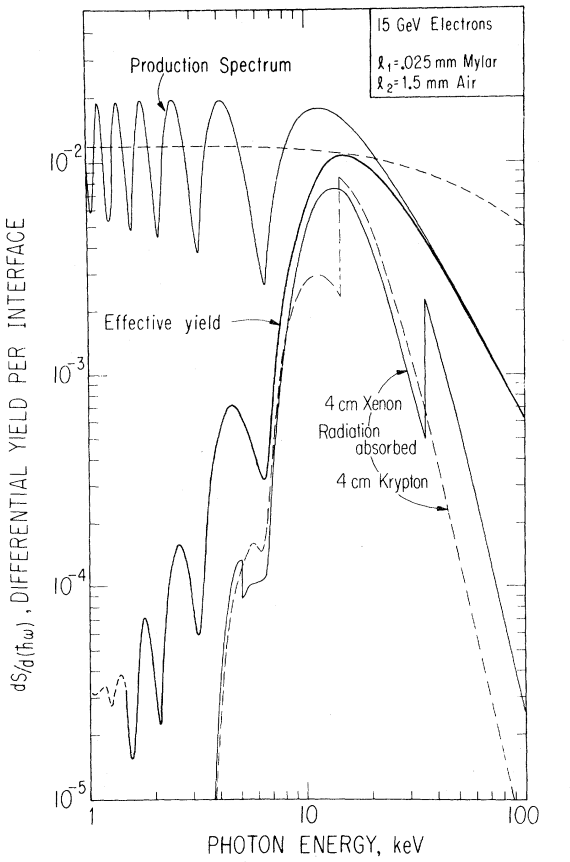

FIG. 4. Comparison of the generated differential yield of a multifoil radiator (production spectrum) with the yield emerging after taking absorption in the radiator into account (effective yield). The strong suppression of low x-ray energies due to absorption should be noted. The lower curves indicate the fraction of the effective yield that will be absorbed in detectors of 4-cm xenon (solid line) or 4-cm krypton (dashed line).

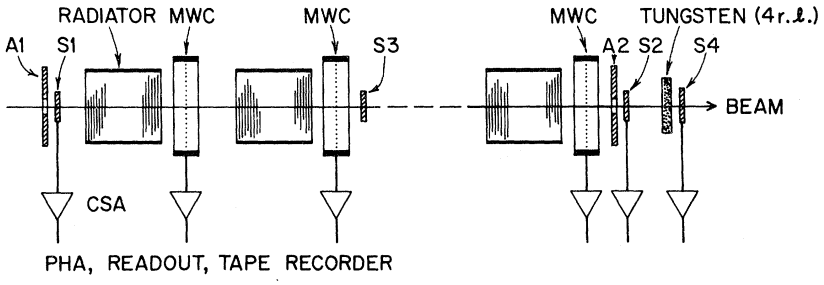

FIG. 5. Schematic diagram of the experimental setup for the accelerator runs. $S1$, $S2$, $S3$ are the beam defining counters, together with the anticounters $A1$, $A2$. $S4$ is a shower counter to identify electrons. Up to seven sets of radiator-multiwire chamber (MWC) pairs were used. The signals were measured with charge-sensitive amplifiers (CSA), digitized with pulse-height analyzers (PHA), and stored on magnetic tape.

lated by bremsstrahlung, δ rays, etc., or by contaminations of the electron beam. However, no noticeable difference between the data obtained with solid targets and without any material in front of the chambers could be observed. Also, at SLAC, measurements were performed with pions of 3 to 15 GeV traversing the detector system. As expected, no transition radiation could be observed due to the much lower Lorentz factors of the pions.

For runs with radiators, frequently a solid piece of plastic material was inserted *behind* a multiwire chamber and in front of the following radiator (see Fig. 5). This reduced the possibility that a photon produced in one radiator might pass through one multiwire chamber and a second radiator before being absorbed in the second chamber. While for a practical detector this feedthrough might mean a welcome increase in the observed signal, for the purpose of this paper, we have selected only those results which are free of feedthrough.

The proportionality of the chambers was checked and the energy calibration was defined with x-ray sources (Fe^{55}, Co^{57}), the 5.9-keV line of Fe^{55} being used as the main energy standard. These calibrations were frequently performed throughout the runs in order to account for long time drifts in the chamber gain. The measured ionization loss (no radiators) of pions and electrons is smaller than expected from tabulated dE/dx values.[21] This difference may be due to the fact that part of the energy is transferred to fast knock-on electrons which can escape from the detection volume ("restricted energy loss"[22]). For instance, the dE/dx values for 1-GeV electrons in krypton chambers (80% Kr, 20% CO_2) or xenon chambers (80% Xe, 20% CO_2) are (in keV/cm):

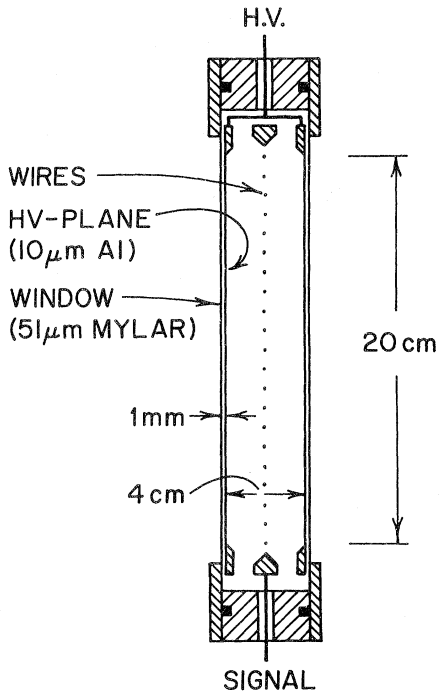

FIG. 6. Schematic cross section of a multiwire proportional chamber.

	$Kr-CO_2$	$Xe-CO_2$
Tables,[21] total dE/dx	7.0	10.0
Tables,[21,22] restricted dE/dx (computed for an escape energy of 50 keV)	4.8	6.9
This measurement	4.1(±5%)	6.7(±5%)

IV. DATA ANALYSIS AND RESULTS

The data obtained in these experiments were processed in the following way: (a) Only events which are characterized by single-electron pulse heights in the scintillation counters $S1$ and $S2$ and which show sufficiently high pulse heights in the shower counter $S4$ have been accepted; (b) slight deviations from linearity in some of the pulse-height analyzers were corrected using electronic calibrations; (c) in order to account for gain drifts of the chambers during the runs (usually less than 10%) the measured pulse heights were normalized using the x-ray calibrations as well as pulse heights from electrons without radiators.

Examples of measured pulse-height distributions are shown in Fig. 7. In each case two distributions are shown, one obtained with a solid target and one with a radiator in front of the chamber. The increase in pulse height (on the average by almost a factor of 2), when electrons pass through a radiator is due to the transition-radiation x rays. The difference of the *average* pulse heights of both distributions for a given configuration defines the *average detected x-ray yield.*

As mentioned above, the x-ray yield is expected to depend critically on a number of experimental parameters. We shall therefore present our results by showing the average detected x-ray yield as obtained for a variety of electron energies and radiator-detector configurations. For each case, we have also calculated the expected yield by a

Monte Carlo method in the following way: For a fixed electron energy and a given radiator, "events" are simulated by computing the number of photons generated (assuming Poisson statistics) and distributing their frequencies according to Eq. (6a). The starting points of the photons are randomly distributed in the radiator. Tabulated absorption cross sections[17-19] are used to determine which of the photons reach the detector and are absorbed there. A possible escape of the fluorescence photon or of the photoelectron is taken into account, as well as fluctuations due to the limited resolution of the detector.

A. Yield versus energy

Figures 8 and 9 exhibit the x-ray yield generated by Mylar targets (188 foils, thickness 25 μm, spacing 1.5 mm) and detected with xenon- or krypton-filled proportional chambers. As can be seen, in this case transition radiation is detectable for electron energies above 1 GeV ($\gamma \approx 2\times10^3$). The yield rises rapidly with energy until saturation is reached between 5 and 10 GeV ($\gamma \approx 1$ to 2×10^4). The error bars quoted arise from uncertainties in the stability of the detector response and from statistical fluctuations. Since the yield is determined by subtracting the averages of two pulse-height distributions (see above), the errors of both averages are taken into account. The calculated yield is indicated by the shaded area. The uncertainty in the calculations is caused by uncertainties in the tabulated x-ray cross sections and by possible inac-

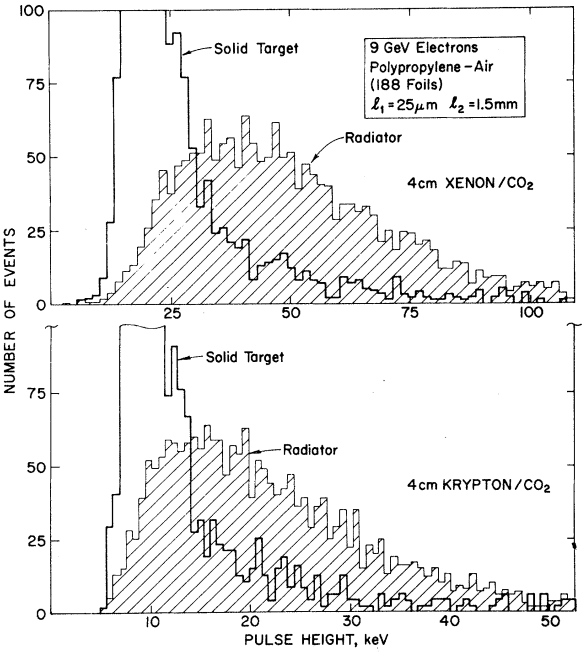

FIG. 7. Pulse-height histograms of the signals measured in a proportional chamber for 9-GeV electrons. The radiator consists of 188 polypropylene foils (l_1 =25 μm), stretched in air (l_2=1.5 mm). The upper spectrum is measured with xenon/CO_2 as detector gas, the lower with krypton/CO_2. Landau-type histograms (heavy lines) are obtained when the radiator is replaced by solid targets of equivalent thickness. All histograms are normalized to the same number of events.

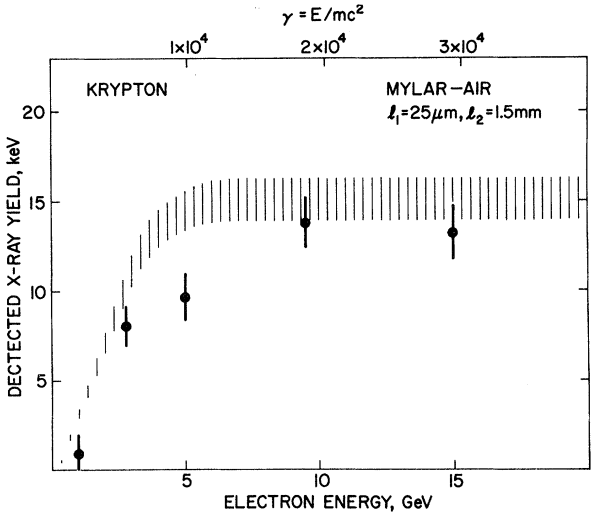

FIG. 8. Detected x-ray yield as function of the electron energy for a radiator consisting of 188 Mylar foils (l_1 =25 μm), stretched in air (l_2=1.5 mm). The data points are measured with a krypton detector, and the shaded region is the result of the computations (the width indicating the computational uncertainty of ± 8%).

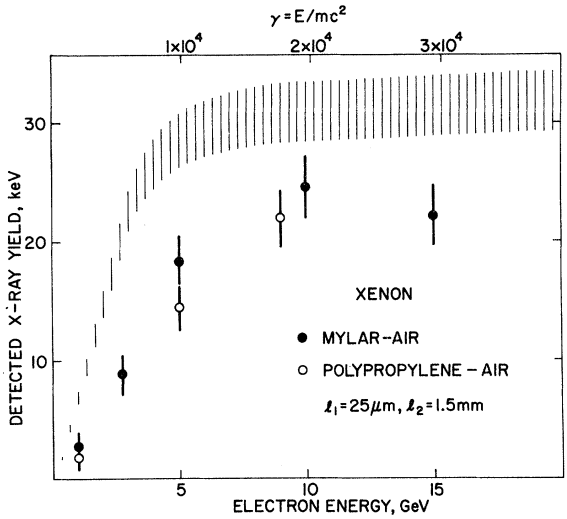

FIG. 9. Same as Fig. 8 for a xenon-filled detector. The solid data points and the shaded region refer to a Mylar radiator, and the open data points have been measured with a polypropylene radiator (188 foils, l_1 =25 μm, stretched in air, l_2=1.5 mm).

curacies in the Monte Carlo program, both errors being of the order ±5%. The results measured with krypton chambers (Fig. 8) agree quite well with the calculations, while in the case of xenon chambers (Fig. 9) the measurements indicate a yield which is about 30% lower than calculated. However, since for xenon the calculated and the measured yields also show the same trend with energy, and because of the possibility of some systematic error, we cannot interpret this discrepancy as serious evidence for questioning the theoretical basis of the calculations.

Figure 9 also shows some data points obtained with polypropylene radiators. The lower plasma frequency of this material as compared to that of Mylar is expected to lead to a shift of the radiation spectrum to lower frequencies. According to Eq. (9) we obtain $\hbar\omega_{max} = 12$ keV for Mylar, and $\hbar\omega_{max} = 8.8$ keV for polypropylene (the foil thickness being in both cases $l_1 = 25$ μm). On the other hand, polypropylene is more transparent to low-energy x rays than Mylar. The calculations show that the two effects essentially balance each other, and that the *detected* radiation yield should be the same for both materials. This agrees well with the observations.

B. Yield versus foil thickness

With increasing foil thickness, the probability of reabsorption of x-ray photons in the radiator increases. However, this effect is offset by the hardening of the radiation: The frequency ω_{max} around which most of the emission occurs is proportional to the foil thickness [see Eq. (9)]. Therefore one expects an increase in the total transition-radiation yield with increasing foil thickness (compare Fig. 3). The *detected* yield will, however, rise only until ω_{max} becomes so large that the x rays are no longer efficiently absorbed in the detector. This expectation agrees well with the measurements, as shown in Fig. 10 for 10-GeV electrons. As an example, for a 50-μm Mylar radiator, $\hbar\omega_{max}$ is about 24 keV, and at this energy only ~29% of the x rays will be absorbed in a 4-cm krypton-CO_2 detector.

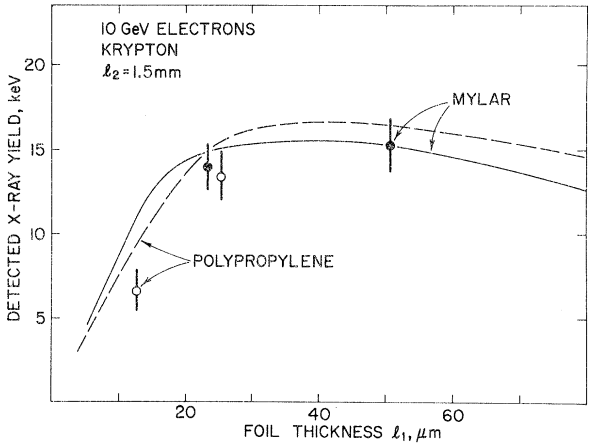

FIG. 10. Detected x-ray yield in krypton/CO_2 chambers as function of foil thickness (188 foils) for 10-GeV electrons. The foil spacing in air is $l_2 = 1.5$ mm. The measured values (open points for polypropylene, full points for Mylar radiators) are compared with the calculations (dashed line for polypropylene, solid line for Mylar radiators). It is interesting to note that the formation zones Z_1 for 15-keV x rays are 20 μm for Mylar and 27 μm for polypropylene (at $\gamma = 2 \times 10^4$).

C. Yield versus air spacing

In Fig. 11 we plot the detected radiation yield for 15-GeV electrons as a function of the air spacing between the radiator foils. Again the agreement between the calculated and the measured yield is much better for krypton than for xenon. As expected, the yield drops sharply if the air spacing is less than 1–2 mm. This is due to the fact that then the saturation energy γ_s [Eq. (8)] becomes less than 15 GeV and the air formation zone Z_2 [see Eq. (3b)] becomes significantly larger than the spacing l_2. For instance, $Z_2 = 8$ mm for 15-keV x rays at $\gamma = 3 \times 10^4$.

D. Yield versus radiator length

Figure 12 shows the measured radiation yield as a function of the length, i.e., the number of foils

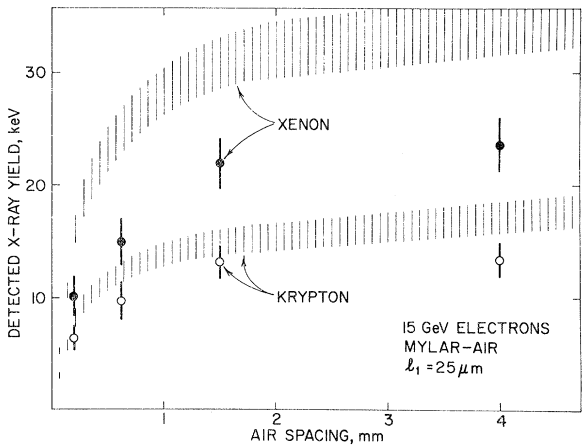

FIG. 11. Detected x-ray yield for 15-GeV electrons as function of the spacing of the foils for Mylar radiators (188 foils, $l_1 = 25$ μm). The solid data points are measured with xenon/CO_2 detectors, and the open points with krypton/CO_2. The shaded regions are the results of the corresponding computations (including the computational uncertainty). The formation zone Z_2 is in this case 8 mm for 15-keV x rays.

of the radiator. Obviously, the yield can increase with the length of the radiator until a limit due to reabsorption of the x rays is reached.

As a further test of the validity of the theoretical calculations on transition radiation, we have compared the measured with the computed pulse-height *distributions*, which include, of course, the ionization signals of the electrons. An example is shown in Fig. 13. No adjustment of the energy scale or of any parameters has been made except that we demand the most likely pulse heights due to the ionization loss (no transition radiation) be the same for the measured and for the calculated data. Within statistical errors, the measured and the calculated distributions are in excellent agreement.

V. DISCUSSION AND CONCLUSIONS

In general, the transition-radiation yield as measured in these experiments confirms the theoretical predictions quite well even though the calculated yields tend to slightly exceed the experimental values. The characteristic dependence of the yield on the configuration of the radiator (i.e., on foil thickness and spacing) has also been observed by other investigators[23,24] and strongly suggests the importance of interference phenomena in multifoil radiators, as discussed in Sec. II. Still, we should point out that our experiments are a somewhat indirect test of the theory. For each set of parameters (energy, radiator configuration, detector properties) only integral measurements have been presented. Our experiments could not resolve the structure of the transition-radiation spectra as shown in Figs. 1, 2, and 4.

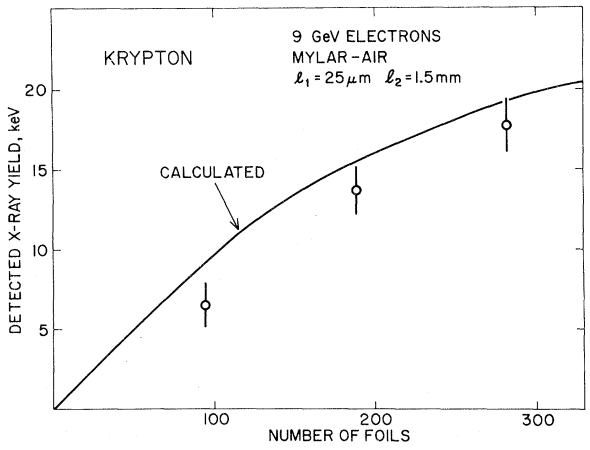

FIG. 12. Detected x-ray yield for 9-GeV electrons as function of the number of foils for a Mylar radiator (l_1 =25 μm, stretched in air, l_2=1.5 mm) measured with a krypton-filled proportional chamber, and compared with the computation.

This measurement remains an important test to be performed in the future.

However, it appears that we are able to calculate by the methods described in this report the transition-radiation yield of multifoil radiators with an absolute accuracy of at least 20–30%. Since our results, as obtained by varying a number of experimental parameters, show in no case a strong deviation of the measured from the calculated behavior, we feel confident in applying the theory to predict the performance of transition-radiation detectors for practical purposes. Such detectors will function with good efficiency if a number of parameters are carefully taken into account, the most important being the following:

(a) Energy of the particle. For the radiators used in our experiments, the radiation yield will saturate at energies slightly above $\gamma = 10^4$ (compare Figs. 3, 8, 9). Below saturation, the *total* yield will be approximately proportional to γ. It is difficult to shift the saturation point to much higher energies. This follows from Eq. (8): For a given radiator material, the saturation energy can be raised by increasing the foil thickness l_1, or the spacing l_2. Increasing l_1 leads to a hardening of the radiation (see below) which is in general not desirable, while an increase of l_2 is possible only as long as the radiator dimensions can be kept within reasonable limits. The total x-ray intensity that can be reached with practical radiators, for instance, of the kind used in our experiments, is relatively small. Therefore, the efficient detection of transition radiation will be restricted to energies around and above saturation, or at most one order of magnitude below the saturation level.

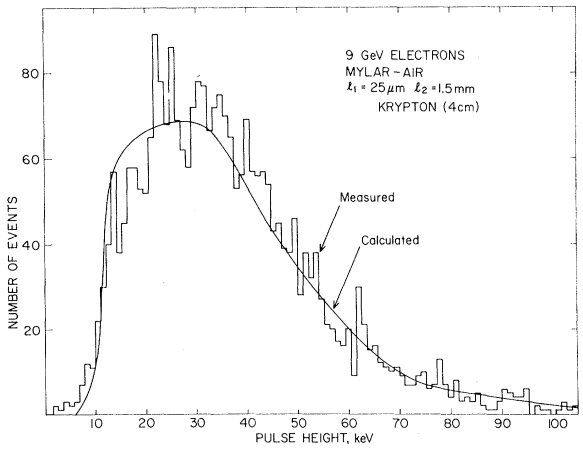

FIG. 13. Comparison of measured and calculated pulse-height distributions for 9-GeV electrons traversing a Mylar radiator (188 foils, l_1=25 μm, l_2=1.5 mm). The detector gas is krypton/CO_2.

(b) Frequency range of the emitted radiation and properties of the detector. As mentioned before, most of the transition x rays are emitted with frequencies around ω_{max} [see Eq. (9)] if the energy of the particle is close to or beyond the saturation energy γ_s [Eq. (8)]. A detector must therefore be used which is highly efficient for x rays in this region. For instance, the gas counters used in our experiments fulfill this criterion quite well, if 25-μm Mylar radiators with $\hbar\omega_{max} = 12$ keV are used.

Care should be taken that the number of x-ray photons per particle in this frequency range is not too small. For most of our experiments, about 2 photons/event have been detected. In general, the higher ω_{max} is chosen (by increasing l_1), the smaller will be the number of photons per frequency interval at ω_{max}.

(c) Materials and dimensions of the radiator. In the range $\gamma\omega_2 < \omega < \gamma\omega_1$ the differential radiation yield is approximately proportional to $\ln(\gamma\omega_1/\omega)$ [see Eq. (2b)]. Therefore, the radiator foils should consist of a material with a large plasma frequency ω_1, that is, a material of high density. However, the x rays will be quickly reabsorbed unless low-Z materials are chosen. Thin plastic foils appear to be an inexpensive compromise and have therefore been used for our experiments. As described under (b), the foil thickness l_1 should be such that the frequency ω_{max} is beyond the range of significant reabsorption in the radiator and coincides with the sensitive region of the detector.

We should stress again the condition $\omega_{max} < \gamma\omega_1$; that is, transition radiation can be expected only in a frequency region well below a "cutoff" frequency $\gamma\omega_1$. This fact becomes especially important if the detection of transition radiation from particles of relatively low energy, e.g., with $\gamma \lesssim 10^3$, is sought. Since $\hbar\omega_1$ is of the order of 10 eV for most suitable radiators, the radiation will be fairly soft, of the order of a few keV, in this case. Care must then be taken that the radiator stays transparent for soft x rays, and radiator materials of as low an atomic number as possible, for instance, lithium or beryllium, should be used.[25]

On the other hand, as discussed above, if a radiator is required that leads to as high a saturation energy γ_s as possible, the spacing l_2 between individual foils is a limiting parameter. This is equivalent to the condition that the formation zone Z_2 should not significantly exceed the foil spacing. For instance, for 15-keV x rays and $\gamma = 10^4$, the formation zone is 2.2 mm in air and 2.6 mm in vacuum. For $\gamma = 10^5$, the respective numbers are 1.1 cm and 26 cm.[26]

Apart from practical limitations, the optimum over-all length of a radiator is exclusively determined by reabsorption of the transition x rays and depends therefore on the radiator material as well as the frequency of the radiation. A 25-μm Mylar radiator of ~1000 foils would lead to a major increase in yield, by a factor of about 2.5, as compared to the detected yield of the radiators (188 foils) typically used in our experiments.

Finally, for a quick estimate of the properties of radiators such as those used in our experiments, the following list of approximate relations might be useful:

(1) The emitted radiation for particle energies greater than or not much below γ_s has frequencies around $\omega_{max} = l_1\omega_1^2/2\pi c$.

(2) The saturation energy is $\gamma_s = E_s/mc^2 = \omega_1 l_2/4\pi c$.

(3) The foil formation zone is $Z_1(\omega) \lesssim 4c\omega/\omega_1^2$.

(4) The gap formation zone is $Z_2(\omega) = (2c\gamma^2/\omega) \times (1+\gamma^2\omega_2^2/\omega^2)^{-1}$.

(5) The above parameters are correlated as follows: $Z_1(\omega_{max}) \approx l_1$; $Z_2(\gamma_s, \omega_{max}) \lesssim l_2^2/4\pi l_1$.

These statements are valid under the following conditions:

$l_1\omega_1^2 \gg l_2\omega_2^2$	(i.e., the mass density of the foils is larger than that of the gap material);
$l_2 \gg l_1$	(i.e., the spacing is much larger than the foil thickness);
$\omega < \gamma\omega_1$	(i.e., frequencies below the cutoff frequency $\gamma\omega_1$ are observed).

Note added in proof. Good agreement between the detected and the calculated transition-radiation yields of multifoil radiators has also been reported by Ellsworth *et al.*[27]

ACKNOWLEDGMENTS

We greatly appreciate the help of the staff of our laboratory and we wish to thank in particular W. Johnson for the mechanical design, D. Bonasera for the electronics work, and N. Beck for contributions to the data handling. S. Jordan has assisted us during the accelerator runs, and we are grateful to Professor I. Lerche for illuminating discussions. Finally, the services, hospitality, and assistance extended to us by the staff of the Stanford Linear Accelerator Center, in particular Dr. R. Gearhart, and of the Cornell Synchrotron, in particular Professor J. DeWire, Dr. M. Tigner, and Dr. J. Humphrey, are gratefully acknowledged.

APPENDIX: DERIVATION OF THE DIFFERENTIAL YIELD FOR MULTIFOIL RADIATORS

We consider a configuration of N parallel foils with dielectric constant ϵ_1 and thickness l_1, spaced at distances l_2 in a medium of dielectric

constant ϵ_2 (see Fig. 14). We wish to calculate the intensity of transition radiation generated when a highly relativistic particle passes perpendicularly through the stack of foils.

The field amplitudes at some observation point P should simply be the coherent sum of the radiation amplitudes from $2N$ single interfaces. The phase factor must be properly included, taking into account that the particle traverses different interfaces at different times.

For a single interface, the x-ray *intensity* has been given in Eq. (1) (Sec. II). The corresponding electric *field amplitude* in the wave zone is, according to Garibian,[13] as follows:

Case (a): Particle passing from medium 1 into medium 2,

$$E_{12} = \frac{A(\theta)}{R} e^{i\varphi}, \tag{A1a}$$

where

$$A(\theta) = e\beta\xi \sin\theta \cos\theta / \pi c R,$$

$$\varphi = \omega\left(\frac{R}{c} - t\right),$$

$$\xi = 2(\epsilon_2 - \epsilon_1)\Big/\left[\left(\frac{1}{\gamma^2} + \theta^2 + \frac{\omega_1^2}{\omega^2}\right)\left(\frac{1}{\gamma^2} + \theta^2 + \frac{\omega_2^2}{\omega^2}\right)\right],$$

θ = emission angle of the photon with respect to the particle trajectory,

R = distance to P,

t = time.

Case (b): Particle passing from medium 2 into medium 1,

$$E_{21} = -E_{12} = -\frac{A(\theta)}{R} e^{i\varphi}. \tag{A1b}$$

The total field amplitude at the point P is obtained by coherent addition, using the fact that the field amplitudes from successive interfaces alternate in sign [by Eqs. (A1a) and (A1b)]:

$$E(P) = \sum_{k=1}^{2N} \frac{(-1)^k A(\theta_k) e^{i\varphi_k}}{R_k}, \tag{A2}$$

where φ_k is the phase factor for radiation from the kth interface, R_k is the distance from the interface to P, and θ_k is the angle between the particle trajectory and the direction of P. If P is sufficiently far from the stack of foils, then we may use the far zone approximation:

$$R_k \approx R, \quad \theta_k \approx \theta \text{ for all } k.$$

Then Eq. (A2) becomes

$$\begin{aligned} E(\theta, R) &= \frac{A(\theta)}{R} \sum_{k=1}^{2N} (-1)^k e^{i\varphi_k} \\ &= \frac{A(\theta)}{R}\left[e^{i\varphi_1} \sum_{k=0}^{N-1} e^{i(\varphi_{2k+1} - \varphi_1)} - e^{i\varphi_2} \sum_{k=1}^{N} e^{i(\varphi_{2k} - \varphi_2)}\right]. \end{aligned} \tag{A3}$$

It can be seen from the geometry of Fig. 14 that the phase difference $\Delta\varphi = \varphi_{k+2} - \varphi_k$ between any two successive even-numbered or successive odd-numbered interfaces is a constant independent of k, and therefore

$$\varphi_{2k} - \varphi_2 = \varphi_{2k-1} - \varphi_1 = (k-1)\Delta\varphi. \tag{A4}$$

Explicitly, we have (taking spatial and temporal separation into account)

$$\Delta\varphi = \frac{\omega}{c}\left[(l_1\sqrt{\epsilon_1} + l_2\sqrt{\epsilon_2})\cos\theta - \frac{l_1 + l_2}{\beta}\right]. \tag{A5}$$

Using Eq. (A4) and substituting into Eq. (A3), we find

$$E(\theta, R) = \frac{A(\theta)}{R}(e^{i\varphi_1} - e^{i\varphi_2}) \sum_{n=0}^{N-1} e^{in\Delta\varphi}. \tag{A6}$$

With

$$\begin{aligned} \sum_{n=0}^{N-1} e^{in\Delta\varphi} &= \frac{e^{iN\Delta\varphi} - 1}{e^{i\Delta\varphi} - 1} \\ &= e^{i(N-1)\Delta\varphi/2} \frac{\sin(N\Delta\varphi/2)}{\sin(\Delta\varphi/2)} \end{aligned} \tag{A7}$$

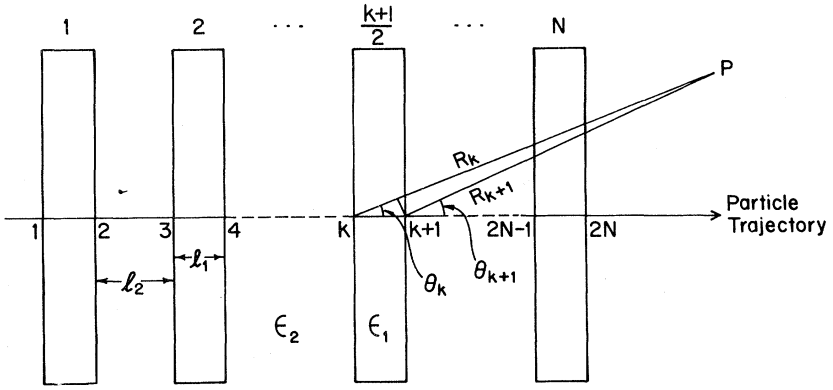

FIG. 14. Schematic diagram of a multifoil radiator.

and after some further manipulations, Eq. (A6) becomes

$$E(\theta, R) = \frac{A(\theta)}{R} e^{i(\varphi_1+\varphi_2+\pi)/2} e^{i(N-1)\Delta\varphi/2} \times 2\sin\left(\frac{\varphi_1-\varphi_2}{2}\right)\frac{\sin(N\Delta\varphi/2)}{\sin(\Delta\varphi/2)}. \quad \text{(A8)}$$

By the same arguments, an analogous expression can be obtained for the magnetic field amplitude H. In order to calculate the differential radiation intensity at the point P the Poynting vector must be computed, and we obtain

$$\frac{d^2S_N}{d\theta d\omega} = \frac{c}{4\pi}\int_{-\infty}^{\infty}\int_0^{2\pi} EH^* R^2 \sin\theta\, d\phi\, dt = \frac{d^2S_0}{d\theta d\omega} 4\sin^2\left(\frac{\varphi_1-\varphi_2}{2}\right)\frac{\sin^2(N\Delta\varphi/2)}{\sin^2(\Delta\varphi/2)}, \quad \text{(A9)}$$

where $d^2S_0/d\theta d\omega$ is the differential yield for a single interface [see Eq. (1a), Sec. II].

It remains to express $\Delta\varphi$ and $(\varphi_1-\varphi_2)/2$ explicitly in terms of the relevant parameters. Using Eq. (A5) and the approximations $\beta = 1 - 1/2\gamma^2$, $\cos\theta = 1 - \theta^2/2$, and $\sqrt{\epsilon_{1,2}} = 1 - \omega_{1,2}^2/2\omega^2$, we find

$$|\Delta\varphi| = \frac{\omega}{2c}\left[l_1\left(\frac{1}{\gamma^2}+\theta^2+\frac{\omega_1^2}{\omega^2}\right)+l_2\left(\frac{1}{\gamma^2}+\theta^2+\frac{\omega_2^2}{\omega^2}\right)\right] = 2\left(\frac{l_1}{Z_1}+\frac{l_2}{Z_2}\right), \quad \text{(A10)}$$

where $Z_{1,2}$ are defined as in Eq. (3b) (Sec. II). Similarly

$$\frac{|\varphi_1-\varphi_2|}{2} = \frac{l_1}{Z_1}. \quad \text{(A11)}$$

The final result is obtained by substituting (A10) and (A11) in Eq. (A9):

$$\frac{d^2S_N}{d\theta d\omega} = \frac{d^2S_0}{d\theta d\omega} 4\sin^2\left(\frac{l_1}{Z_1}\right)\frac{\sin^2[N(l_1/Z_1+l_2/Z_2)]}{\sin^2(l_1/Z_1+l_2/Z_2)}. \quad \text{(A12)}$$

---

*Work supported in part by the National Aeronautics and Space Administration under Grants Nos. NGL 14-001-005 and NGR 14-001-224.

†NATO Postdoctoral Fellow at the Enrico Fermi Institute, on leave from Physikalisches Institut, Universität Bonn, Germany.

[1]V. L. Ginzburg and I. M. Frank, Zh. Eksp. Teor. Fiz. 16, 15 (1946).

[2]G. M. Garibian, Zh. Eksp. Teor. Fiz. 33, 1403 (1957) [Sov. Phys.—JETP 6, 1079 (1958)].

[3]M. L. Ter-Mikaelian, Nucl. Phys. 24, 43 (1961).

[4]P. Goldsmith and J. V. Jelley, Philos. Mag. 4, 836 (1959).

[5]F. R. Arutunian, K. A. Ispirian, and A. G. Oganessian, in *Proceedings of the International Conference on High Energy Physics, Dubna, 1964,* edited by Ya. A. Smorodinskii *et al.* (Atomizdat, Moscow, U.S.S.R., 1966), p. 933.

[6]J. Oostens, S. Prünster, C. L. Wang, and L. C. L. Yuan, Phys. Rev. Lett. 19, 541 (1967).

[7]L. C. L. Yuan, C. L. Wang, and S. Prünster, Phys. Rev. Lett. 23, 496 (1969).

[8]L. C. L. Yuan, C. L. Wang, H. Uto, and S. Prünster, Phys. Lett. 31B, 603 (1970).

[9]A. I. Alikhanian, S. A. Kankanian, A. G. Oganessian, and A. G. Tamanian, Phys. Rev. Lett. 30, 109 (1973).

[10]F. Harris, T. Katsura, S. Parker, V. Z. Peterson, R. W. Ellsworth, G. B. Yodh, W. W. M. Allison, C. B. Brooks, J. H. Cobb, and J. H. Mulvey, Nucl. Instrum. Methods 107, 413 (1973).

[11]M. L. Cherry, D. Müller, and T. A. Prince, Nucl. Instrum. Methods 115, 141 (1974).

[12]M. L. Ter-Mikaelian, *High-Energy Electromagnetic Processes in Condensed Media* (Wiley, New York, 1972).

[13]G. M. Garibian, Zh. Eksp. Teor. Fiz. 39, 332 (1960) [Sov. Phys.—JETP 12, 237 (1961)].

[14]G. M. Garibian, Zh. Eksp. Teor. Fiz. 60, 39 (1971) [Sov. Phys.—JETP 33, 23 (1971)].

[15]The justification for approximation (5) is complicated by the fact that the period of the function $\sin^2(l_1/Z_1 + l_2/Z_2)$ in Eq. (3a) can be comparable to the period of $\sin^2(l_1/Z_1)$. It can be shown, but is beyond the purpose of this paper, that approximation (5) can also be used in this case.

[16]The integration of Eq. (3a) to obtain Eq. (6a) depends on the validity of replacing the term $\sin^2[N(l_1/Z_1+l_2/Z_2)]/\sin^2(l_1/Z_1+l_2/Z_2)$ by a sum of δ functions

$$N\pi\sum_{k=-\infty}^{\infty}\delta[(l_1/Z_1+l_2/Z_2)-\pi k].$$

This substitution is valid under the condition that the width of the "spikes" of $\sin^2[N(l_1/Z_1+l_2/Z_2)]/\sin^2(l_1/Z_1+l_2/Z_2)$ be small compared to the range over which $(d^2S_0/d\theta d\omega)\sin^2(l_1/Z_1)$ varies considerably. See G. M. Garibian, in Proceedings of the International Conference on Instrumentation for High Energy Physics, Frascati, 1973 (unpublished), p. 329; Yerevan Physical Institute Scientific Report No. EFI 27 (73), 1973 (unpublished); V. I. Zatsepin, in *Proceedings of the Thirteenth International Conference on Cosmic Rays, Denver, 1973* (Colorado Associated Univ. Press, Boulder, 1973), Vol. 4, p. 2842. This leads to the requirement

$$N(l_1+l_2) > \frac{4\pi c}{\omega}\left(\frac{1}{\gamma^2}+\frac{\omega_2^2}{\omega^2}\right)^{-1} = \pi Z_2(\theta=0).$$

This condition is fulfilled in most practical cases.

[17]B. L. Henke, R. L. Elgin, R. E. Lent, and R. B. Ledingham, Norelco Reporter 14, 112 (1967).

[18]E. Storm and H. I. Israel, Los Alamos Scientific Lab-

oratory Report No. LA-3753, 1967 (unpublished).
[19]W. H. McMaster, N. Kerr-del Grande, J. H. Mallett, N. E. Scofield, R. Cahill, and J. H. Hubbell, Lawrence Radiation Laboratory Report No. UCRL-50174, 1968 (unpublished).
[20]T. Prince, D. Müller, G. Hartmann, and M. L. Cherry, Nucl. Instrum. Methods (to be published).
[21]Nuclear Science Series Report No. 39, NAS-NRC Publ. 1133, 1967 (unpublished).
[22]M. J. Berger and S. M. Seltzer, in Ref. 21, p. 205.
[23]L. C. L. Yuan, C. L. Wang, H. Uto, and S. Prünster, Phys. Rev. Lett. 25, 1513 (1970).
[24]L. C. L. Yuan, in *Proceedings of the Twelfth International Conference on Cosmic Rays, Hobart, 1971*, edited by A. G. Fenton and K. B. Fenton (Univ. of Tasmania Press, Hobart, Tasmania, 1971), Vol. 4, p. 1499.
[25]J. Fischer, S. Iwata, V. Radeka, C. L. Wang, and W. J. Willis, Phys. Lett. 49B, 393 (1974).
[26]In order to arrive at numerical values for $Z_{1,2}(\theta,\omega)$ according to Eq. (3b) we set $\theta^2=(1/\gamma^2+\omega_2{}^2/\omega^2)$.
[27]R. Ellsworth, J. MacFall, G. Yodh, F. Harris, T. Katsura, S. Parker, B. Peterson, L. Shiraighi, B. Stenger, J. Mulvei, B. Brooks, and J. Cobb, in *Proceedings of the Thirteenth International Conference on Cosmic Rays, Denver, 1973* (Colorado Associated Univ. Press, Boulder, 1973), Vol. 4, p. 2819.